Available online at www.sciencedirect.com

ScienceDirect

Energy Procedia 1 (2009) 4945–4952

Energy Procedia

www.elsevier.com/locate/procedia

GHGT-9

Topographic effects on CO_2, diffusion and dissolution from the seafloor

Kristin Rygg[a,b,] *, Lars Inge Enstad[a,b], Guttorm Alendal[b,c], Peter Mosby Haugan[a]

[a] *Geophysical Institute, University of Bergen, Allégaten 50,5007 Bergen, Norway*
[b] *Bergen Centre for Computational Science, Unifob, Høyteknologisenteret, Thormöhlensgate 55,5008 Bergen, Norway*
[c] *Department of Mathematics, University of Bergen, Johannes Brunsgate 12, 5008 Bergen, Norway*

Abstract

At 3000 meters depth liquid CO_2 is denser than seawater and hence will be stored as a "lake" on the deep ocean floor, which is expected to gradually be dissolved in seawater. Ocean currents and turbulence will influence the net rate of dissolution by several orders of magnitude compared to molecular diffusion. On the other hand, density stratification induced by dissolved CO_2 will tend to dampen the local turbulence and reduce the vertical mixing. It is well known that local topography will alter the currents and turbulence intensity, and hence, change the dissolution rates. Earlier the dissolution of a CO_2 lake has been studied through idealized 3D simulations with a flat bottom using MITgcm coupled with GOTM. This new study includes how topographic depressions affect the dissolution rate and gives also a comparison of how the different coordinate systems affect the results. The lake scenario is modeled in a two dimensional domain using the terrain following coordinate model, Bergen Ocean Model, (http://math.uib.no/BOM/) and the *z*-coordinate MIT general circulation model (http://mitgcm.org).

Keywords: CO_2; ocean; storage; sigma model; z-coordinate; CO_2 lake;

1. Introduction

The global concentration of CO_2 in the atmosphere is increasing due to burning of fossil fuel. In order to reduce the emissions of CO_2 to the atmosphere, several sequestration methods have been suggested. No single sequestration method will be able to solve the climate problem, and in order to reduce the CO_2 concentrations in the atmosphere to preindustrial levels; several mitigation strategies must be used [1]. The ocean covers approximately 70% of the Earth's surface, and there is a balance between the CO_2 levels in the atmosphere and in the sea. Whether the CO_2 is first released into the atmosphere or the water column, the concentrations in the atmosphere will eventually reach the same levels [2]. However, in general the time when the CO_2 is isolated from the atmosphere increases with the

* Corresponding author. Tel.: +47-555-84075; fax: +47-555-84295.
E-mail address: Kristin.Rygg@bccs.uib.no.

doi:10.1016/j.egypro.2009.02.326

injection depth in the water column [2], and the delay in time before the injected CO_2 is released into the atmosphere might be a contributor to help provide a bridge to a society based on renewable energy sources. On the other hand, such an injection of CO_2 into the water column will affect marine organisms and might have ecosystem consequences. However, presently there is a net flux of CO_2 into the world oceans, some 1 million tons of CO_2 per hour [3], causing acidification at the most productive upper layer [4].

The present article shows results from simulations of a CO_2 lake located at 3000 meters depth. Since CO_2 is more compressible than water, at this depth CO_2 is denser than seawater and will form lakes at the bottom of depressions. The scenario will also be applicable for dissolution of CO_2 reaching the benthic boundary layer from beneath, i.e. leaks of geologically stored CO_2. The simulations presented here are 2D studies performed with a σ-coordinate model, Bergen Ocean Model, and a *z*-coordinate model, the MIT general circulation model.

2. The governing equations

In order to simulate the diffusion and dissolution of CO_2 from the seafloor two ocean models have been used, the MIT general circulation model and Bergen Ocean Model (BOM). The MITgcm is a *z*-coordinate model [5], while BOM uses terrain following coordinates [6]. Both models use the Boussinesq approximation, and the momentum equations may be written as follows,

$$\frac{\partial U}{\partial t}+\frac{\partial U^2}{\partial x}+\frac{\partial UW}{\partial z}=-\frac{1}{\rho_0}\frac{\partial P}{\partial x}+\nu\left(\frac{\partial^2 U}{\partial x^2}+\frac{\partial^2 U}{\partial z^2}\right), \tag{1}$$

$$\frac{\partial W}{\partial t}+\frac{\partial UW}{\partial x}+\frac{\partial W^2}{\partial z}=-\frac{1}{\rho_0}\frac{\partial P}{\partial z}-\frac{\rho g}{\rho_0}+\nu\left(\frac{\partial^2 W}{\partial x^2}+\frac{\partial^2 W}{\partial z^2}\right). \tag{2}$$

For an incompressible fluid, the equation of continuity may be expressed as,

$$\frac{\partial U}{\partial x}+\frac{\partial W}{\partial z}=0. \tag{3}$$

Additionally a conservation equation for scalar quantities, ϕ, as salinity, temperature and CO_2 is needed,

$$\frac{\partial \phi}{\partial t}+\frac{\partial U\phi}{\partial x}+\frac{\partial W\phi}{\partial z}=K\left(\frac{\partial^2 \phi}{\partial x^2}+\frac{\partial^2 \phi}{\partial z^2}\right). \tag{4}$$

In the equations above *U(x,z,t)* represents horizontal velocity, *W(x,z,t)* vertical velocity, *P(x,z,t)* the pressure, $\rho(x,z,t)$ the density, ρ_0 a reference density, and *g* the constant of gravity. In order to close the system, values for the eddy viscosity, ν, and the eddy diffusivity, *K,* must be chosen.

Neither MITgcm nor BOM in their standard versions includes the tracer CO_2. The CO_2 signal is dynamically active, since the density of seawater increases with higher CO_2 concentrations. The new equation of state can be expressed as,

$$\rho_{mix}=\rho(S,T,p,CO_2)=\rho(S,T,p)+[M_{CO_2}-\rho(S,T,p)\nu_{CO_2}]C_T, \tag{5}$$

which is the same equation as used in previous CO_2 lake studies [7, 8 ,9,10]. In Equation (5) the concentration of CO_2 is represented by C_T [mol m^{-1}], the molar mass M_{CO2}=44.01x10^{-3} kg mol^{-1}, and ν_{CO2}=34x10^{-6} m^3 mol^{-1} is a conservative (high) estimate of the molar volume of CO_2.

In order to simulate the CO_2 lake, a source term is located at the bottom boundary. In this study we have not included the effect of hydrate formation. The CO_2 flux is expressed by [7, 8, 9, 10],

$$J_{CO_2}=\frac{1}{1-\widetilde{C}_s}\left[K_m\frac{\rho_s}{M_s}(\widetilde{C}_s-\widetilde{C}_{amb})\right], \tag{6}$$

where $C_s = 35\text{x}10^{-3}$ is the solubility of CO_2 in seawater (mole factor), C_{amb} the concentration of CO2 in the ambient water (mole factor), and the density of water saturated with CO_2 is represented by ρ_s [kg m^{-3}]. The molar mass of the dissolved CO_2 in seawater is calculated according to,

$$M_s = M_w(1-\widetilde{C}_s) + M_{CO_2}\widetilde{C}_s. \quad (7)$$

The mass transfer coefficient K_m is given by $K_m = 0.1u^* \text{Sc}^{-0.67}$, where Sc is the Schmidt number set to 10^3, and u^* is the friction velocity,

$$u_* = \frac{\kappa}{\ln\frac{0.5\Delta z_1 + z_0^b}{z_0^b}}\sqrt{(U_1^2 + V_1^2)}, \quad (8)$$

where $V_1 = 0$. The lateral velocity is zero since the present study is 2 dimensional and without rotation. In Equation (8), κ represents the Von Karman constant set to 0.4, z_0^b represents the surface bottom roughness, and Δz_1 the distance from the bottom to the nearest grid point. At the bottom there is a bottom drag, specified by,

$$\vec{\tau}_x = \rho_0 C_D |U_b| U_b, \quad (9)$$

where the drag coefficient C_D is represented by,

$$C_D = \frac{\kappa^2}{(\ln\frac{z_b}{z_0})^2}. \quad (10)$$

3. Model setup

The simulations are simplified 2 dimensional simulations. The equations are discretized on a domain with length 19.5 km, and 200 meter vertical extent. The lake is located at 3000 metes depth, but only the lowest 200 meters of the water column is included in the model. Three topographic scenarios have been chosen; in the first the CO_2 lake is located at a flat bottom, and in the second and third, the lake is located in a cleft with a depth of 10 meters or 20 meters. A simple step function to define the topography is implemented in MITgcm, and in BOM a tanh-function is used.

The grid resolutions are equidistant both in the horizontal and in the vertical directions, with a horizontal resolution of 75 meters. For the *z*-coordinate model, the vertical resolution is 2 meter, and for the σ-coordinate

Table 1. The simulations presented in this paper.

Simulation number	Model	Topography [m]	Vertical viscosity and diffusivity [$m^2 s^{-1}$]	Horizontal diffusivity [$m^2 s^{-1}$]
1	MITgcm	0	10^{-2}	10
2	MITgcm	10	10^{-2}	10
3	MITgcm	20	10^{-2}	10
4	MITgcm	0	10^{-6}	10
5	MITgcm	10	10^{-6}	10
6	MITgcm	20	10^{-6}	10
7	BOM	0	10^{-2}	10
8	BOM	10	10^{-2}	0
9	BOM	20	10^{-2}	0
10	BOM	0	10^{-6}	10
11	BOM	10	10^{-6}	0
12	BOM	20	10^{-6}	0

model, the vertical extent is divided into 100 σ-layers, leading to a vertical resolution varying between 2 meters and 2.2 meters depending on the total depth of the domain. The CO_2 lake, with length 500 meters, is located 5.5 km from the upstream boundary in a homogeneous environment with a density of 1025 kg m^{-3}, and a background velocity of 0.1 m s^{-1} in the interior. The lake itself is located below the lower boundary of the model, and only the flux of dissolved CO_2 from the surface of the lake is included in the model. Periodic boundary conditions are used in the horizontal direction. The simulations are run for 12 hours before the CO_2 flux is turned on, this in order to ensure a fully developed velocity profile.

In order to close the system, values for the eddy viscosity and diffusivity must be chosen. In these simulations constant horizontal and vertical eddy viscosities and diffusivities are used. Two different vertical eddy diffusivities and viscosities are used, 10^{-2} m^2 s^{-1} and 10^{-6} m^2 s^{-1}, while in the horizontal the eddy viscosity and diffusivity is set to 10 m^2 s^{-1}. However, in the simulations with topography with BOM, the horizontal eddy diffusivity is set to 0 m^2 s^{-1}. This choice is made in order to avoid unphysical mixing related to the terrain-following coordinate system [6, 11, 12]. Table 1 gives an overview over the simulations presented in this paper. In all the simulations the hydrostatic approximation has been used.

4. Results

Figure 1 shows a snapshot of the CO_2 concentration, the horizontal velocity profile, and the vertical velocities after 35 hours, (23 hours after the release time for the CO_2 flux) for Simulation 1 and 7 (Table 1). Both models seem to capture the same maximum values for concentration, horizontal velocity, and vertical velocity.

The volumes of water masses with concentrations larger than four threshold values, 0.1 mol m^{-3}, 1 mol m^{-3}, 5 mol m^{-3}, and 10 mol m^3, are presented in Figure 2. The simulations with high vertical eddy viscosities and diffusivities give very small differences in the volumes of the water masses. In the simulations with vertical eddy viscosities and diffusivities of 10^{-6} m^2 s^{-1}, larger differences occur, both in volumes and in the magnitudes of the concentrations. In

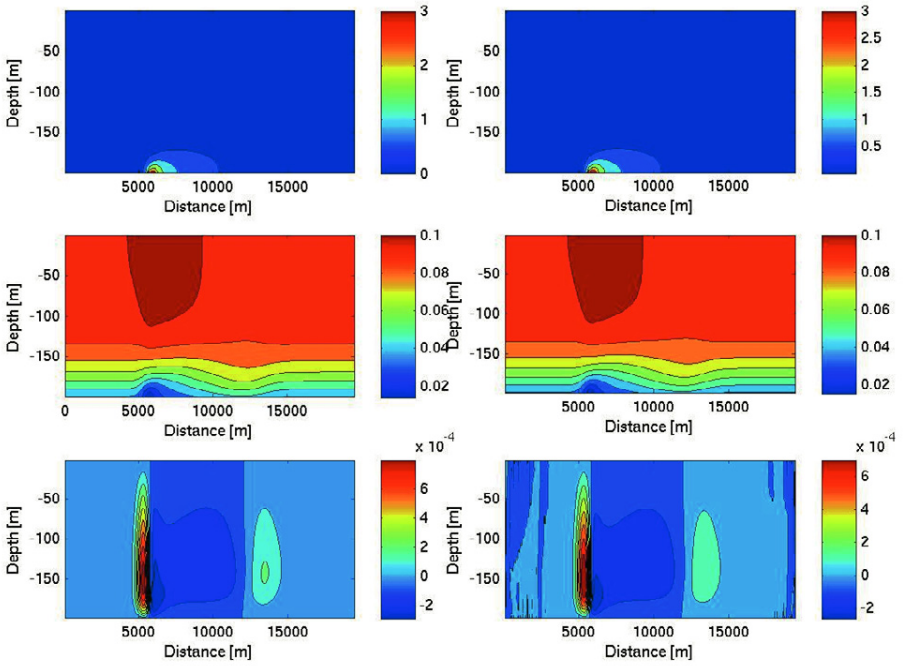

Figure 1. Snapshots of CO_2 concentration, horizontal velocity, and vertical velocity after 35 hours (23 hours after the CO_2 flux is turned on). The left column gives results from Simulation 1 (MITgcm), and the right column gives results from Simulation 7 (BOM).

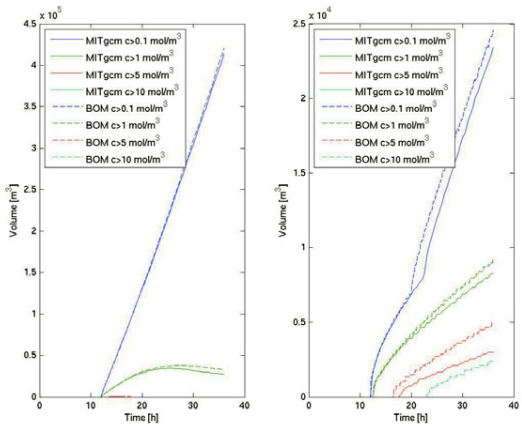

Figure 2. Volume of water masses with a concentration higher than 0.1 mol m^{-3}, 1 mol m^{-3}, 5 mol m^{-3}, and 10 mol m^{-3}. The left figure shows results from the simulations with flat bottom and high viscosities (Simulation 1 and 7). The right figure shows results from the simulations with flat bottom and low viscosities (Simulation 4 and 10).

the simulations using low viscosities in Figure 2, a breaking point may be observed for the volume of water masses with a concentration higher than 0.1 mol m^{-3} after approximately 20 hours. The increase in the gradient coincides with the time when the water masses with a concentration larger than 0.1 mol m^{-3} reaches above the boundary layer.

In Figure 3 and Figure 4 important characteristics as mean CO_2 concentration in the first grid level above the lake, total amount of CO_2 in the model (mol) and volume of water masses with a concentration larger than 0.1 mol m^{-1} are compared for the three topographic scenarios. Introducing topography in the domain reduces both volume and total mass of CO_2 in the water column above and downstream the lake. This is valid for both BOM and MITgcm.

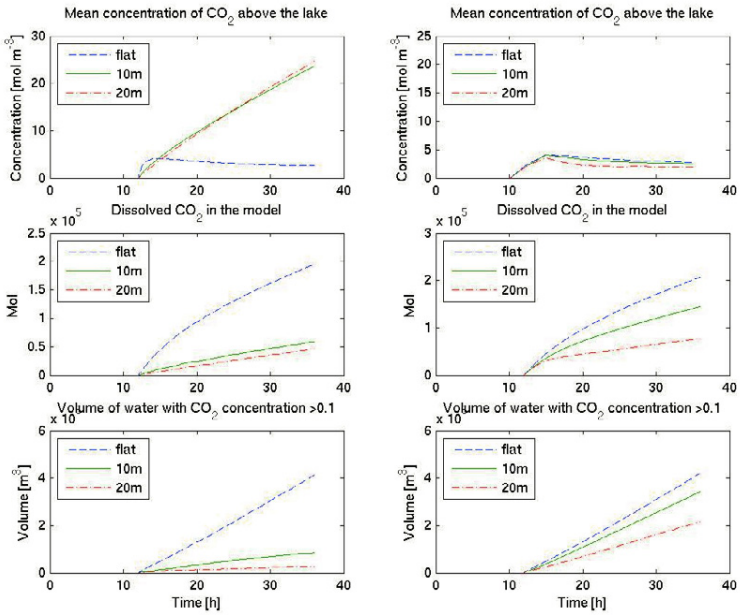

Figure 3. Mean CO_2 concentration over the lake, mass of CO_2 in the domain measured in mol, and total volume in the model of water masses with a concentration higher than 0.1 mol m^{-3}. In the left column the results from Simulation 1-3 (MITgcm) are presented and in the right column the results from Simulation 7-9 are presented (BOM).

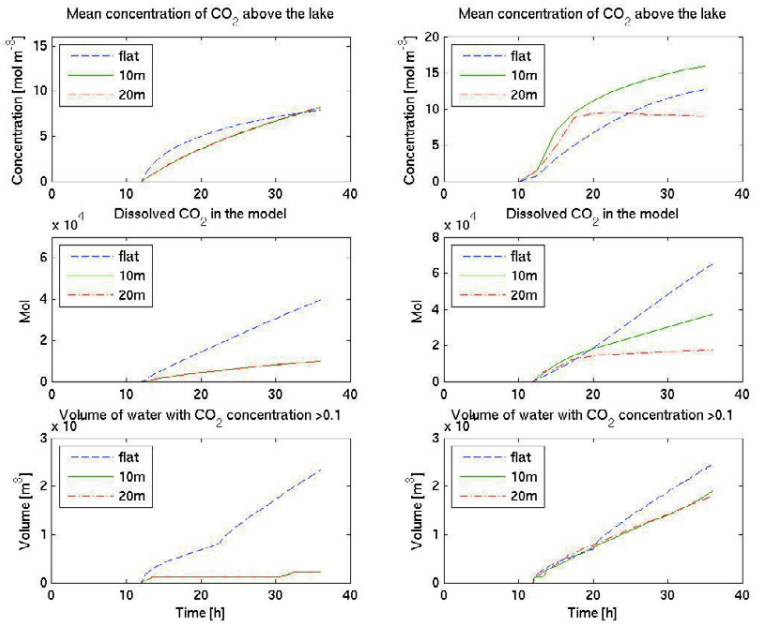

Figure 4. Mean CO_2 concentration over the lake, mass of CO_2 in the domain measured in mol, and total volume in the model of water masses with a concentration higher than 0.1 mol m^{-3}. In the left column the results from Simulation 4-6 (MITgcm) are presented and in the right column the results from Simulation 10-12 are presented (BOM).

Increasing the depth of the trench increasingly reduces the volume of water with a CO_2 concentration above a certain threshold and total mass of dissolved CO_2 with time. The reductions are quite different by using a terrain following model compared to a *z*-coordinate model. The *z*-coordinate model gives much smaller volumes affected by the lake than the σ–coordinate model. In the low viscosity simulations with MITgcm (Simulation 5 and 6) there are very small differences in mass of CO_2 in the model and volume masses affected depending on the topography (Figure 4). When it comes to the magnitude of the CO_2 concentration above the lake, there is no general tendency in increase or decrease with depth of the trench.

Table 2 The average flux from the CO_2 lake. In each time step the CO_2 flux is averaged above the lake At the end of the simulation the CO_2 flux from each time step is averaged from the time when the flux is quasi-stable (12 hours after the CO_2 flux is turned on) and to the end of the simulation. The last column gives the dissolution rate for the 12 simulations, calculated from the CO_2 flux in Column 5.

Simulation number	Model	Topography [m]	Vertical viscosity and diffusivity [$m^2 s^{-1}$]	Flux CO_2 lake [µmol $cm^{-2} s^{-1}$]	Dissolution rate [cm yr^{-1}]
1	MITgcm	0	10^{-2}	0.31	415
2	MITgcm	10	10^{-2}	0.11	147
3	MITgcm	20	10^{-2}	0.10	129
4	MITgcm	0	10^{-6}	0.08	109
5	MITgcm	10	10^{-6}	0.11	147
6	MITgcm	20	10^{-6}	0.10	129
7	BOM	0	10^{-2}	0.34	452
8	BOM	10	10^{-2}	0.23	307
9	BOM	20	10^{-2}	0.01	14
10	BOM	0	10^{-6}	0.15	203
11	BOM	10	10^{-6}	0.21	279
12	BOM	20	10^{-6}	0.10	134

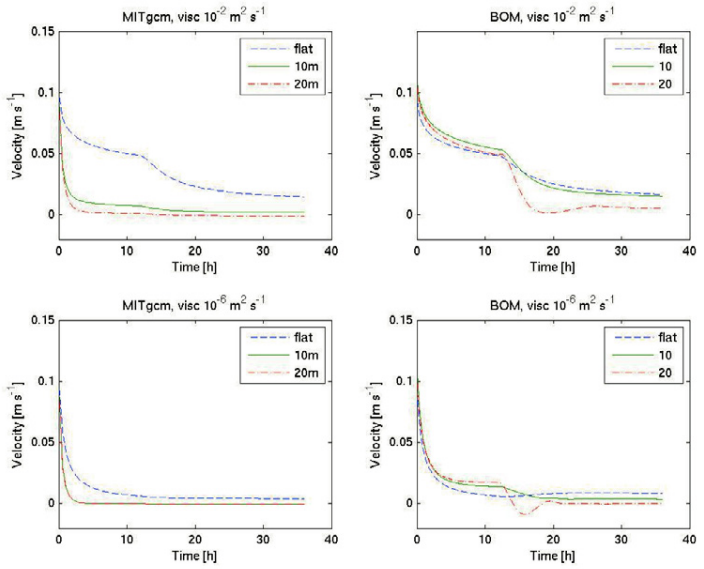

Figure 5. Mean velocity over the lake. The left figure at the top gives results from Simulation 1-3 (MITgcm), the right figure at the top gives results from Simulation 7-9 (BOM), the lower figure at the left presents the mean velocities from Simulation 4-6 (MITgcm), while the figure at the bottom to the right gives results from Simulation 10-12 (BOM).

In Figure 5 the mean velocity over the lake is presented. The mean velocities at the bottom of the trench are more affected by the topography in MITgcm than in BOM (first 12 hours in Figure 5). In the cases with 10 meter deep topography, the mean velocity over the lake in MITgcm is approximately half the mean velocity in BOM. The mean velocity is more affected by the introduction of the CO_2 flux in the σ-coordinate model than in the z-coordinate model. Note that in Simulation 10, the mean velocity increases after the CO_2 flux is turned on, leading to a higher friction velocity, and then a higher flux into the model. This can explain why there is more mass of CO_2 in Simulation 10 than in Simulation 4. Additionally observe how the small differences in mean velocity for Simulation 5 and 6 are related to approximately the same volumes and masses in Figure 4.

Table 2 gives the average value of the flux from the CO_2 lake throughout the simulation. For the high viscosity cases the flux is reduced with increasing depth of the cleft. However in the low viscosity cases the results are more chaotic. The CO_2 flux and the volumes increase with increasing vertical eddy viscosities and diffusivities (Figure 3, Figure 4, and Table 2).

5. Summary and discussions

For the scenario with high vertical viscosities and a flat bottom, the agreement between the two models is very good compared to what is found in similar model-model comparisons on oceanic scales. For these simulations (Simulation 1-3 and 7-10) there are quite clear indications that the volumes of the water masses affected by the CO_2 lake and the CO_2 flux is reduced by locating the CO_2 lake in a trench. However, for the simulations using molecular values for vertical viscosities and diffusivities there are no clear correlation between flux, and topography for neither MITgcm nor BOM. With viscosities and diffusivities of this scale more small scale motion is allowed, and the lacking correlation might be due to unresolved processes. Previous studies of these two models have shown a convergence in the results also for these values of vertical viscosities and diffusivities. However, these studies were done with a very small grid resolution (ΔX~2mm) [13]. In Berntsen et. al. (2006) [13] they observed that the solutions were less diffusive in the MITgcm. This result corresponds with our study, with higher values of CO_2 in Simulation 10 than in Simulation 4. The resolution in this study is 75 meters and it has been chosen to use the

hydrostatic approximation. At these scales non-hydrostatic features might be important [14], and it would be interesting in the future to study if higher resolution and using a non-hydrostatic pressure solver would lead to a clearer correlation regarding volumes affected, and CO_2 flux and location of the lake.

By introducing topography in the domain, quite large differences occur between the two ocean models. BOM gives a higher flux rate than MITgcm in most cases, most likely mainly due to the higher velocities in the bottom of the trench caused by the coordinate system. Terrain-following models are known to create artificial flow due to internal pressure errors, and iso-pycnal diffusion [6]. Hence BOM might overestimate the mixing and give a too large inflow flux. On the other side, by using a z-coordinate model for this kind of a study, the velocities in the lowest grid cells of the cleft is only weakly affected by the ambient velocity field, leading to too low velocities and an unphysical small inflow flux. The mean velocity at the bottom of the cleft is an important parameter in order to achieve the correct fluxes and by that the affected water masses.

In the future we will extend the study to include estimates of the mixing based on an advanced turbulence mixing scheme from the General Ocean Turbulence Model [15, 16]. We will also make considerations on the horizontal diffusivity scheme in the σ-coordinate model in order to take the coordinate system into account in a more sophisticated manner.

6. Acknowledgements

The work is funded by the EU project CARBOOCEAN.

7. References

1 S. Pacala and R. Socolow, (2004), Stabilization Wedges: Solving the Climate Problem for the next 50 Years with Current Technologies, Science, 305, 968-972.
2 IPCC, (2005), Special Report on Carbon Dioxide Capture and Storage. Prepared by Working Group III of the Intergovernmental Panel on Climate Change. Cambridge University Press.
3 P. G. Brewer, (2007), Evaluating a technological fix for climate, Proc Natl Acad Sci USA, 104, 9915-9916.
4 K. Caldeira and M. E. Wickett, (2003), Anthropogenic carbon and ocean pH, Nature, 425.
5 A. Adcroft et al. , (2008), MITgcm User Manual.
6 J.Berntsen, (2004), USERS GUIDE for a modesplit σ-coordinate numerical model. Technical Report 4.1.
7 I. Fer and P. M. Haugan, (2003), Dissolution from a liquid CO_2 lake disposed in the deep ocean, Limnology and Oceanography, 48(2), 872-883.
8 P. M. Haugan and G. Alendal, (2001), Turbulent diffusion and transport from a CO_2 lake in the deep ocean, J. Geophys. Res, 110.:C09S14.
9 L. I. Enstad, P. M. Haugan, and G. Alendal, (2006),Dissolution of CO_2 from the sea-floor to oceanic waters. Proceedings of the 8th International Conference on Greenhouse Gas Control Technologies.
10 L. I. Enstad, K. Rygg, G. Alendal, and P. M. Haugan, (2008), Dissolution from a CO_2 lake modeled by using an advanced vertical turbulence mixing scheme, International Journal of Greenhouse Gas Control, Special Issue.
11 W. Huang and M. Spaulding, (2002), horizontal diffusion errors in σ-coordinate coastal ocean models with a second-order Lagrangian-interpolation finite-difference scheme, Ocean Engineering, 29, 495-512.
12 G. Zängl, (2002), Notes and Correspondence, An Improved Method for Computing Horizontal Diffusion in a Sigma-Coordinate Model and Its Application to Simulations over Mountainous Topography, Monthly Weather Review, 1423-1432.
13 J. Berntsen, J. Xing, and G. Alendal, (2006), Assessment of non-hydrostatic ocean models using laboratory scale problems, Continental Shelf Research, 26, 1433-1447.
14 J. Marshall, C. Hill, L. Perelman, and A. Adcroft, (1997), Hydrostatic, quasi-hydrostatic, and nonhydrostatic ocean modeling, J. Geophys. Res, 102: C3, 5733-5752.
15 H. Burchard, (2002), Applied Turbulence Modelling in Marine Waters, Lecture Notes in Earth Sciences, ISBN 3-540-43795-9, Springer.
16 L. Umlauf, H. Burchard, K. Bolding, GOTM Sourcecode and Test Case Documentation, Version 4.0.